Article:
Sharma, H., Chakinala, N., Thota, C. et al. (2 more authors) (2026) Exploring the Catalytic Conversion of Pyrolytic Wax Residue: Kinetics and Co-Pyrolysis. Journal of Analytical and Applied Pyrolysis, 193 (Part 2). 107331. ISSN: 0165-2370

https://doi.org/10.1016/j.jaap.2025.107331

Exploring the Catalytic Conversion of Pyrolytic Wax Residue: Kinetics and Co-Pyrolysis

Himanshi Sharma[1, 2], Nandana Chakinala[1,3*], Chiranjeevi Thota[4], Daya Shankar Pandey[5], Anand Gupta Chakinala[1*]

[1]*Chemical Reaction Engineering Laboratory, Department of Biotechnology & Chemical Engineering, Manipal University Jaipur, Jaipur - 303007, Rajasthan, India*

[2]*Department of Biosciences, Manipal University Jaipur, Jaipur, 303007, Rajasthan, India*

[3]*School of Chemistry, University of Leeds, Leeds, LS2 9JT, United Kingdom*

[4]*Bharat Petroleum Corporation Limited (BPCL), Corporate Research & Development Centre, Greater Noida, Uttar Pradesh, 201306, India*

[5]*School of Mechanical Engineering, University of Leeds, Leeds, LS2 9JT, United Kingdom*

**Corresponding author: anandgupta.chakinala@jaipur.manipal.edu*

n.chakinala@leeds.ac.uk

ABSTRACT:

This study explores the valorization of pyrolysis waxy residue (PWR), a semi-solid byproduct remaining after the distillation of lighter fractions from paper and plastic waste derived pyrolysis oil, with the aim of optimizing hydrocarbon production. Three strategies were assessed: (1) co-pyrolysis of PWR with sawdust (SD) at varying ratios, (2) catalytic pyrolysis using molecular sieves (MS) and ZSM-5 catalysts, and (3) catalytic co-pyrolysis combining PWR, SD, and catalysts. Thermal decomposition analysis of the PWR revealed maximum volatile release, with complete conversion achieved at 550 °C. Kinetic parameters were estimated using Coats Redfern method and the activation energy was found in the range of 31.3 – 38.9 kJ mol^{-1} (avg: 35.3 kJ mol^{-1}). Non catalytic fixed-bed co-pyrolysis at the optimum temperature of 550 ˚C showed a 3:1 PWR-to-SD ratio maximizing the hydrocarbon content (79.0%) but resulted in low oil yields of (~13%,). In contrast, catalytic pyrolysis of PWR with MS resulted in a significantly higher hydrocarbon

yield with negligible phenolic compounds, while ZSM-5 enhanced the gas production to 32.5% but slightly reduced hydrocarbon yield to 65.9%. Catalytic co-pyrolysis using MS provided higher oil yields of ~40% with hydrocarbon content at 71.0%. Despite the challenge of converting long-chain hydrocarbons into oily sludge, the findings highlight the potential for complete conversion and maximized liquid yields through catalysts and co-pyrolysis with biomass mixtures.

Keywords: *Pyrolysis waxy residue; Zeolites; Molecular sieves, ZSM-5, Hydrocarbons, Kinetics*

1. Introduction

Plastics are now an integral part of life that are produced in a massive scale worldwide to produce a large variety of products that are consumed every day but also generates a large volume of waste that end up without being treated. Only a few selected plastics are currently being recycled while most of them (~70%) ends up as a plastic waste. It is forecasted that the global plastic production will be tripled and is expected to generate around 12 billion tons of plastic wastes by 2050[1]. There are several options available for the treatment of these plastic wastes such as feedstock recycling, mechanical recycling, energy recovery and incineration. However, these processes have their limitations in terms of techno-economics and the environmental concerns associated with the processes [2] [3]. Therefore, cost effective technologies are needed to convert these wastes to useful products.

Pyrolysis is a mild thermal treatment process which can effectively break down the molecules in the absence of oxygen to liquid, gas fuels and solid char. However, pyrolytic liquid products from non-catalytic pyrolysis are often unsuitable for direct use and require further refinement. Depending on the operating conditions and feed characteristics, pyrolysis of mixed plastic waste under non-catalytic conditions generates solid wax residues up to ~47% that mainly constitute long chain hydrocarbons ($>C_{23}$)[4].

Pyrolysis wax residues (PWR), a heavy by-product from plastic pyrolysis, is typically managed through landfilling, incineration, or solvent extraction, which pose environmental risks and offer limited resource recovery[5]. Recent studies have explored thermochemical methods like pyrolysis and hydrothermal liquefaction for PWR conversion, but these often face low efficiency and high residue formation. Research on catalytic upgrading of real PWR, especially through co-pyrolysis with biomass. Most existing work focuses on synthetic waxes, leaving a gap in understanding the

behavior of complex, real-waste residues. This study addresses these gaps by evaluating catalytic co-pyrolysis of PWR with biomass to enhance liquid fuel yields and product quality.

In this context, several strategies were proposed in the literature aiming to maximize the desirable liquid product distributions from the pyrolysis of plastic waste by optimizing the process conditions, employing catalysts, pyrolysis reactors with reflux conditions[6]. For instance, a microwave-assisted catalytic pyrolysis of paraffin wax with SiC@HZSM-5 catalyst produced up to ~80 wt.% liquid oil which consisted of ~77% gasoline fractions (57% BTX aromatics), and the gas product had 49% olefins, with less than 2 wt.% residue[7]. Similarly, the catalytic cracking of high-density polyethylene (HDPE) pyrolysis waxes under fluid catalytic cracking (FCC) conditions demonstrated that at higher catalyst-to-oil ratios (7 g g^{-1}), HDPE waxes achieved conversions comparable to or higher than vacuum gas oil (VGO). The naphtha produced from HDPE wax was rich in olefins and n-paraffins but had fewer aromatics compared to VGO. These results highlight the potential of FCC to convert plastic pyrolysis waxes into valuable fuels[8]. Additionally, a study on hydrocracking Fischer-Tropsch (FT) wax using Ni-impregnated hierarchical zeolites (ZSM-5, Beta, H-Y, Mordenite) revealed that the catalyst activity was dependent on the acidic strength, with Ni/desilicated ZSM-5 showing 97.6% eicosane conversion and 84.1% liquid selectivity under optimal conditions. These studies reflect that non-noble metal catalysts can efficiently hydrocrack FT wax into valuable fuel products[9].

Further catalytic cracking of HDPE-wax and PP-wax mixtures at 527°C using FCC-ECAT resulted in propylene yields up to 7-10 wt.%, C_4 hydrocarbons (20-23 wt.%), and gasoline (29-36 wt.%), from HDPE-wax. In comparison, PP-wax cracking produced propylene (4-9 wt.%), C_4 hydrocarbons (15 - 24 wt.%), and higher gasoline yields (31 - 48 wt.%) than HVGO cracking, with similar product composition[10]. In a different study, catalytic hydrocracking of pyrolyzed waste

plastic wax using Hβ and Pd/Hβ catalysts. Hβ achieved 64% wax conversion with 98% saturated and unsaturated hydrocarbons in the naphtha. Pd/Hβ enhanced conversion to over 97.5% at 360°C, producing primarily saturated hydrocarbons. Pd [0.6]/Hβ gave 99.2% conversion and 97.8% naphtha. Catalyst deactivation occurred due to coking on acid sites after repeated use. The study highlights the potential of Pd/Hβ for converting waste plastic wax into valuable naphtha-range hydrocarbons[4].

Despite considerable advancements in pyrolysis and catalytic pyrolysis technologies, significant research gaps remain in the catalytic co-pyrolysis of PWR. Most previous studies have focused on cleaner, synthetic plastic waxes rather than real PWR, which is a more complex, heavier by-product with challenging characteristics. Additionally, the co-pyrolysis of PWR with waste biomass under catalytic conditions is rarely explored, and the potential synergistic effects remain unclear. The specific catalytic roles of ZSM-5 and molecular sieves in enhancing product quality and reducing residue from PWR are also not well established in existing literature. Furthermore, limited efforts have been made to optimize process parameters to maximize fuel yields from PWR, which poses several operational challenges in terms of low process efficiencies and environmental risks. Addressing these gaps is essential for developing efficient, scalable solutions for the valorization of pyrolysis by-products.

Although ZSM-5 and molecular sieves are well-known catalysts, this study explores their application to a complex, real PWR derived from paper–plastic pyrolysis distillation. Most previous studies focus on synthetic waxes or pure plastic samples, while this work addresses the catalytic and co-pyrolysis conversion of a heavier, more challenging industrial residue. Additionally, the integration of biomass in co-pyrolysis with PWR remains underexplored. This

combination provides a unique approach to enhance hydrocarbon recovery while offering a sustainable waste management solution.

In this study, wastepaper and plastics obtained from a local industry was converted into pyrolytic liquid in a semi batch rotary kiln pyrolysis unit. The obtained pyrolytic oil was distilled to separate lighter volatile compounds which also resulted in large amounts of bottom PWR after the distillation comprised of high boiling compounds with long chain hydrocarbons. The objective of this study is therefore to explore different conversion strategies of the PWR to produce valuable products. Sawdust was selected as the biomass co-feedstock due to its wide availability, renewability, and high volatile content, which makes it an effective hydrogen donor during co-pyrolysis. Its lignocellulosic structure helps balance the high carbon and low hydrogen content of PWR, improving product quality and liquid fuel yields[11,12]. ZSM-5 and molecular sieves were chosen as catalysts based on their strong acidity, shape selectivity, and proven effectiveness in cracking heavy hydrocarbons and upgrading pyrolysis vapors. Zeolite-based catalysts like ZSM-5 have been widely used in plastic pyrolysis for improving hydrocarbon yields and product selectivity [13][14].

Among available methods, pyrolysis offers a cleaner, energy-efficient, and flexible solution for treating mixed plastic waste. Operating in an oxygen-free environment, it reduces harmful emissions and generates fewer greenhouse gases compared to incineration. Pyrolysis efficiently converts heterogeneous residues like PWR into valuable products such as pyrolysis oil, syngas, and char, while providing higher flexibility in recovering liquid fuels and monomers than mechanical recycling or gasification[5][15,16]. A schematic of the strategies adapted for the maximizing the liquid yields is studied as illustrated in Figure 1.

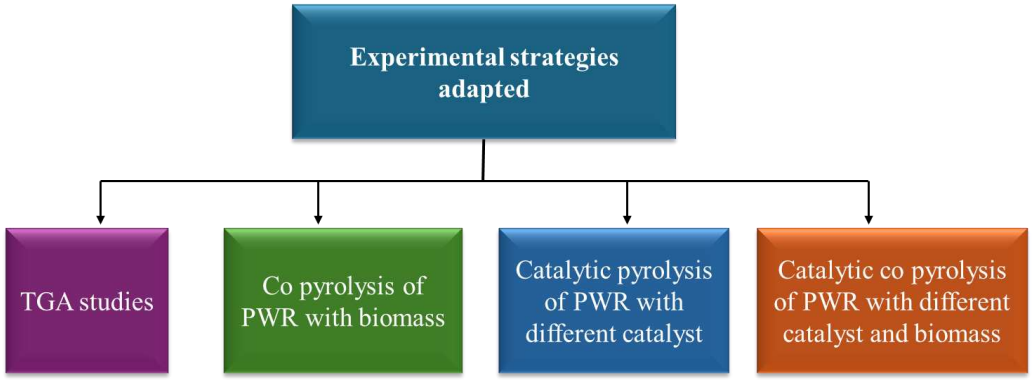

Figure 1: Flowsheet of experimental strategies for the conversion of pyrolytic oil sludge residues.

2. Materials and Methods

2.1 Materials

The PWR feed used in this study was obtained after the distillation of pyrolytic liquid of paper and plastic waste pyrolysis carried out in a semi-pilot rotary kiln reactor at 550 °C[17]. Sawdust (SD) used in the co-pyrolysis experiments was obtained from Sustainable Technologies, Nagpur, India, and was preheated for 1 hour to remove the moisture content.

Molecular sieve catalysts (Molsieve 13X, with a diameter of 1.5 mm) were sourced from Gujarat Multi Gas Base Chemicals, Gujarat, India. A commercial fresh ZSM-5 catalyst was supplied by Bharat Petroleum Corporation Limited (BPCL). All catalysts were preheated in a hot-air oven at 100°C for 1 hour to remove moisture before being used in the experiments.

2.2 Experimental set-up:

The fixed-bed batch pyrolysis reactor utilized in this study is depicted in Figure S1 and is detailed elsewhere [18,19],[20]. The reactor is constructed as a stainless-steel hollow cylinder with an inner diameter of 4 cm, an outer diameter of 6 cm, and a total length of 50 cm. It operates with a heating rate of 35 °C min^{-1} and has a capacity to hold up to 100 g of feed per run. The pyrolysis products are directed through a two-stage glass condenser, where most of the pyrolysis oil is collected from the first stage.

Experiments were organized into three distinct categories, conducted at an optimum temperature of 550°C that was determined in our earlier studies[19,20], Co-pyrolysis: This category involved combining PWR with SD in varying ratios of 1:1, 1:3, and 3:1. Catalytic Pyrolysis: In this step, molecular sieves (MS) and ZSM-5 were used as catalysts at a catalyst-to-feed ratio of 1:1. Catalytic Co-Pyrolysis: This final category combined PWR with SD in the presence of the same catalysts employed in the catalytic pyrolysis, maintaining a catalyst-to-feedstock ratio of 1:1. This

comprehensive experimental design aimed to evaluate the effects of varying feedstock ratios and catalysts on the pyrolysis yields and product composition. Preliminary pyrolysis experiments using PWR alone were also conducted as a control. However, due to its semi-solid and highly sticky nature, the pyrolysis of PWR alone resulted in negligible liquid yield and substantial char formation, which adhered strongly to the reactor walls, making the process unmanageable. To address this, SD was co-fed to improve handling, enhance vaporization, and increase liquid product recovery. Additionally, a catalyst-to-feedstock ratio of 1:1 was selected based on previous trials.[21]

2.3 Analysis methods

The Proximate analysis was performed according to ASTM D7582 and ASTM D3176 standards. Elemental analysis was conducted using a Flash Smart V CHNS analyser from Thermo-Fisher Scientific. Thermogravimetric analysis (TGA) was carried out with a Shimadzu DTG-60H instrument, employing N_2 gas at flow rates between 10 and 50 ml min^{-1}. Fourier Transform Infrared (FTIR) analysis was performed using a Bruker ALPHA FTIR spectrometer with a resolution of 0.8 cm^{-1}.

The composition of the pyrolysis oil was analysed using gas chromatography-mass spectrometry (GC/MS). Prior to analysis, moisture in the oil samples was removed by adding anhydrous sodium sulphate and then filtering the samples. Chromatographic separation was achieved using a Shimadzu GCMS QP2020 series, with the oven temperature programmed from 50 °C (held for 2 min) to 250 °C at a rate of 10 °C min^{-1} and then held at 250 °C for 2 minutes. Helium was used as the carrier gas at a flow rate of 23.9 ml/min, with a split ratio of 15. Powder X-ray diffraction (XRD) analysis was performed using a Rigaku Smart Lab instrument with Cu Kα radiation, scanning within the 10 - 80° range. The morphology and qualitative elemental composition of the

samples were examined using Field Emission Scanning Electron Microscopy (FESEM) with the JEOL JSM-7610 F-Plus instrument. Brunauer-Emmett-Teller (BET) analysis of the fresh catalysts was conducted using a Micromeritics Tristar 3000 V6.08 analyser.

3. Results and discussion

3.1 Feed characterization

3.1.1 Elemental analysis of the feeds

Table 1: CHNS analysis of the PWR and SD on dry basis.

Sample	**C (wt.%)**	**H (wt.%)**	**N (wt.%)**	**S (wt.%)**	**O (wt.%)**	**Total**	**H/C**	**O/C**	**Calorific value (MJ Kg^{-1})**
PWR	84.78	13.21	1.32	0.00	0.68	**100**	1.85	0.01	34.5
SD	44.06	5.41	0.43	0.00	50.10	**100**	1.46	0.85	17.8

The elemental analysis of the two different feeds (PWR and SD) used in this study is shown in Table 1. It is evident from the table that the calorific value of the PWR is double (34.5 MJ kg^{-1}) the value of SD (17.8 MJ kg^{-1}). This significant difference arises from the high carbon content (84.78 wt.%) and low oxygen content (0.68 wt.%) of PWR, which is derived from the pyrolysis of paper and plastic wastes. Plastics, being hydrocarbon-rich polymers, contribute to the higher calorific value and lower oxygen content of PWR compared to SD feedstock characterized by high oxygen content (50.1 wt.%). Additionally, PWR exhibits a higher H/C and lower O/C ratios as compared to SD. These compositional differences of PWR and SD influence their behaviour in pyrolysis and catalytic processes, with PWR being more energy-dense and less oxygenated than SD.

192 *3.1.2 Thermal decomposition and kinetic studies of PWR:*

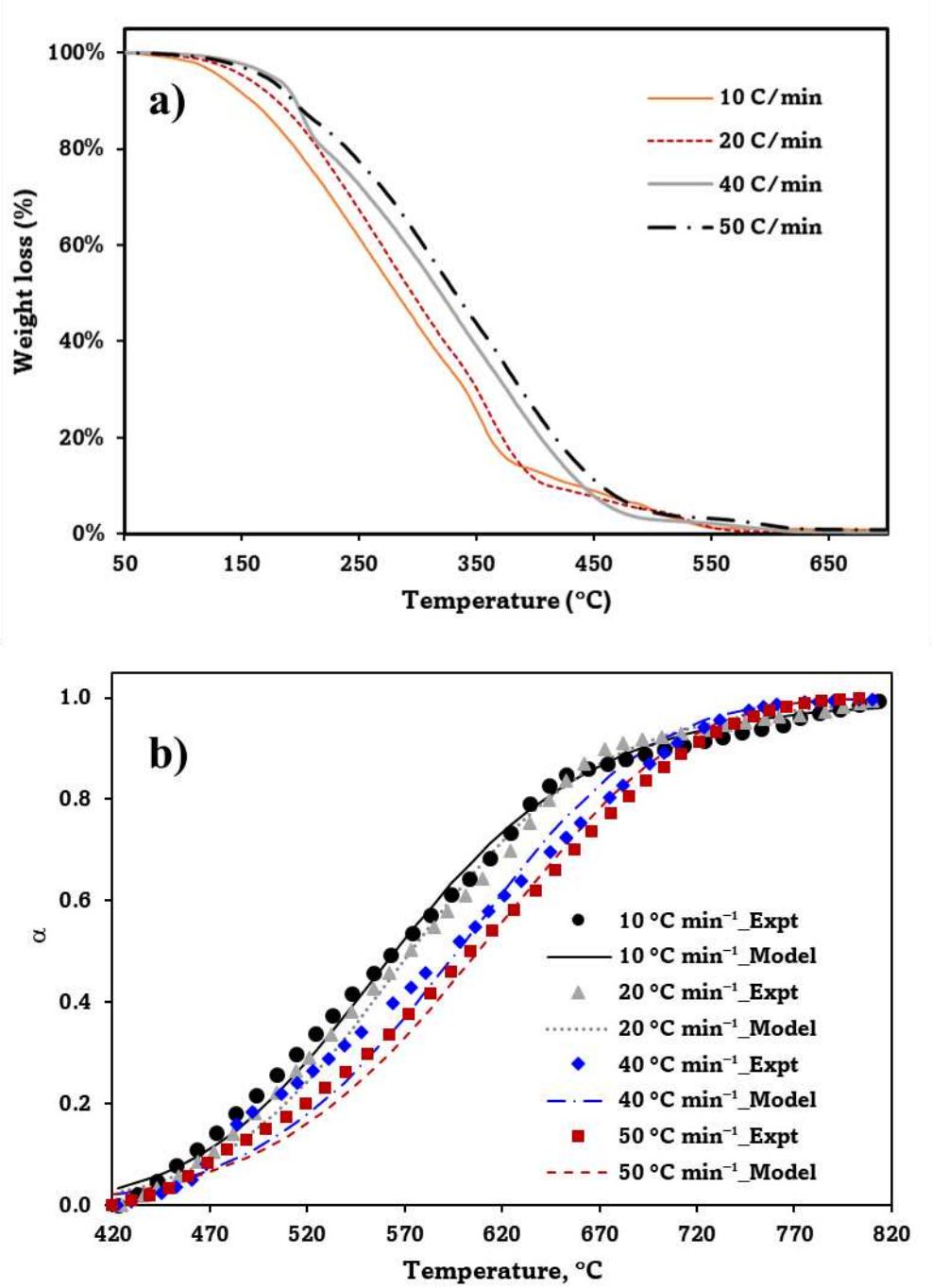

193

194 *Figure 2: Thermal decomposition studies of PWR a) Weight loss profiles of PWR at different heating*

195 *rates b) experimental and model fittings at different heating rates.*

196 Thermal decomposition and kinetic studies of PWR were carried out at different heating rates (10,

197 20, 40 and 50 °C min^{-1}) as shown in Figure 2. It is clear from Figure 2a that the major weight loss

198 profile occurs within the temperature range of 150 – 550 °C and no residue was obtained after this
199 temperature at all the heating rates studied, clearly indicating the presence of maximum volatiles
200 in the PWR which can be recovered. Furthermore, an increase in the heating rate (from 10 to 50
201 °C min^{-1}), notably shifts the thermal decomposition range towards higher temperatures, reflecting
202 the influence of heating rate on the thermal degradation behavior of PWR.
203 The TGA data of the PWR was subsequently analyzed using the Coats Redfern method to estimate
204 the kinetic parameters. Coats Redfern method was proven to exhibit a good fitting of both
205 experimental and model values of conversion of different biomasses that was reported in our earlier
206 studies[19,22]. Hence, this model was adapted in this study to evaluate its feasibility in determining
207 the thermal decomposition kinetics of PWR. Complete details of the model and its algorithm are
208 provided in our earlier study, and it is now briefly presented in equations 1 to 3 below.

$$\frac{\ln g\,(\alpha)}{T^2} = \ln\left(\frac{AR}{\beta E_a}\right) - \left(\frac{E_a}{RT}\right) \quad (1)$$

$$g(\alpha) = \int_0^{\alpha} \frac{d\alpha}{f(\alpha)} \quad (2)$$

$$f(\alpha) = (1-\alpha)^n \quad (3)$$

209 A plot of $\frac{\ln g\,(\alpha)}{T^2}$ versus $\left(\frac{1}{T}\right)$ gives a straight line from which the activation energy (E_a) can be
210 estimated, where n is the order of reaction, A is the frequency factor, T is the temperature, R is the
211 universal gas constant, α is the conversion and β is the heating rate.
212 The TGA data for the active pyrolysis zone in the range of 150 – 550 °C was used to estimate the
213 kinetic parameters using the above method. It is seen that the kinetic parameters such as activation
214 energy and the reaction order were found to decrease with increasing heating rate. The estimated
215 activation energy and reaction order at heating rates of 10, 20, 40 and 50 °C min^{-1} were found to
216 be 37.6, 38. 9, 33.5 and 31.3 kJ mol^{-1} while the reaction order at these heating rates were estimated
217 to be 1.70, 1.55, 1.06, 0.96 respectively. Figure 2b clearly shows a good fitting (R^2>0.96) of the

experimental and obtained model values of PWR conversion in the active pyrolysis zone with different heating rates. The prediction capability of the kinetic model developed shows a good fitting with feeds like oily sludge. Thermal decomposition and kinetic studies of SD carried at different heating rates (30, 40, 50 K min^{-1}) have resulted in the activation energy in the range of 27 – 40 kJ mol^{-1}. The activation energy of SD was estimated using the Coats-Redfern method[19] and are comparatively within the range for PWR. Therefore, the discussion also highlights the suitability of the Coats-Redfern model for accurately analyzing complex feeds such as oily sludge.

3.2 Catalyst characterization

The fresh MS catalyst exhibited a surface area of 572 m^2 g^{-1}, including a micropore area of 498 m^2 g^{-1}, with a micropore volume of 0.18 cc g^{-1} and a total pore volume of 0.30 cc g^{-1}. In comparison, the ZSM-5 catalyst showed a lower surface area of 272 m^2 g^{-1}, a micropore area of 186 m^2 g^{-1}, and a total pore volume of 0.17 cc g^{-1}. The higher surface area of the MS catalyst compared to ZSM-5 correlates with its higher catalytic activity, enabling better access to reactive sites and promoting the production of lighter fractions in the pyrolysis oil.

A comparison of the acidity profiles of two different catalysts MS and ZSM-5 is shown in Table 2. Zeolites possess significant acidity profiles due to the aluminosilicate nature depending on the Si/Al ratio and specific exchange cations. For X-type zeolites (here MS) the Si/Al ratio is lower having higher alumina content indicating higher acid sites.

MS possesses a remarkably high total acidity of approximately 686.2 µmol/g, characterized by a dominant contribution from weak-to-medium strength sites (242.2 °C) alongside a significant proportion of strong acid sites (570.5 °C). In contrast, ZSM-5 exhibits a lower total acidity of about 210.9 µmol/g, predominantly comprising medium-to-strong acid sites (453.6 °C) and a smaller fraction of weak sites. This difference in acidity, combined with their distinct pore structures,

significantly impacts their coking resistance in pyrolysis. MS, with its high acid site density and larger pores, is generally more susceptible to coke formation as it offers ample space for polyaromatic precursor growth and promotes excessive cracking. Conversely, ZSM-5's lower overall acidity and, crucially, its characteristic medium pore size and shape selectivity, sterically hinder the formation of large coke molecules while allowing desired products to diffuse out, thereby imparting superior coking resistance and potentially longer catalyst lifetimes in the co-pyrolysis of biomass and oily sludge residue.

Table 2: Comparative acidity profiles of MS vs. ZSM-5 catalysts.

Sample ID	Brønsted acidity (µmol/g)	Lewis acidity (µmol/g)	Very strong acid sites / defect sites (µmol/g)	Total acidity (µmol/g)
MS	~571.78	~113.61	~0.4	~686
ZSM-5	~16.53	~194.39	-	~211

The FTIR analysis of different catalysts, including fresh and spent MS and ZSM-5 is shown in Figure 3a. The fingerprint regions of fresh and spent MS catalysts were found to be almost identical, as was the case with fresh and spent ZSM-5 catalysts. For MS catalysts, the major peaks were observed at 3756, 1525, 975, 747, and 550 cm^{-1}. The peak at 3756 cm^{-1} was attributed to O-H bonding of hydroxyl groups, while the peak at 1525 cm^{-1} indicated C=C stretching, which was present in both spent catalysts. The peaks in the range of 975 cm^{-1} to 747 cm^{-1} were associated with the stretching vibrations of –NH groups. In the case of both MS and ZSM-5 catalysts, the peak at 550 cm^{-1} corresponds to the bending vibration of SiO_4 and AlO_4 groups. Additionally, for ZSM-5 catalysts, a peak at 1024 cm^{-1} was observed, indicating the external asymmetric stretching of the Si−O−Si bridge[23]. This analysis indicates that the catalytic activity of MS is superior to that of ZSM-5 due to its broader fingerprint region and the presence of more functional groups

261 The XRD patterns of the fresh and spent catalysts (MS and ZSM-5) are presented in Figure 3b,
262 highlighting multiple peaks that confirm the crystalline nature of the materials. For the fresh MS
263 catalyst, prominent diffraction peaks were observed at 2θ values of 6.3, 10.2,12.0, 15.7, 20.3, 23.6,
264 27.0, 31.2, and 33.9°. In comparison, the spent MS catalyst exhibited peaks at 5.6, 7.61, 8.43, 10.4,
265 12.7, 14.3, 15.9, 18.1 and 19.4°. Similarly, the fresh ZSM-5 catalyst displayed peaks at 5.7, 7.7,
266 8.7, 10.4, 12.0, 12.8, 14.5, 15.1, 16.2, and 18.3°. The spent ZSM-5 catalyst showed diffraction
267 peaks at 6.1, 9.0, 10.7, 12.3, 13.1, 14.7, 15.4, 16.5, and 18.6°. These notable changes in the XRD
268 patterns reflect structural changes in the catalysts after use, potentially due to the operating
269 temperatures along with the carbonaceous deposits on the catalyst surface.
270 The SEM images (Figure 3 c & d) displayed the crystalline structure of the spent catalysts,
271 providing valuable insights into their surface morphology. The surface elemental composition of
272 the catalysts was qualitatively determined using EDX analysis, which confirmed the deposition of
273 carbon content. The elemental composition analysis of the catalysts revealed the following
274 distributions: The elemental composition of the spent MS catalysts after the reaction revealed
275 ~57% carbon while, the carbon content on spent ZSM-5 was ~ 30%.
276 Although detailed coke recovery and quantification were not performed due to the limited
277 availability of the feedstock, preliminary signs of coke formation were evident. The FTIR spectra
278 of the spent catalysts showed additional peaks, particularly in the C=C stretching region, indicating
279 the presence of carbonaceous deposits. Similarly, changes in the XRD patterns, including peak
280 shifts and intensity variations in the spent catalysts compared to the fresh ones, further confirmed
281 structural modifications likely caused by coke deposition during pyrolysis.

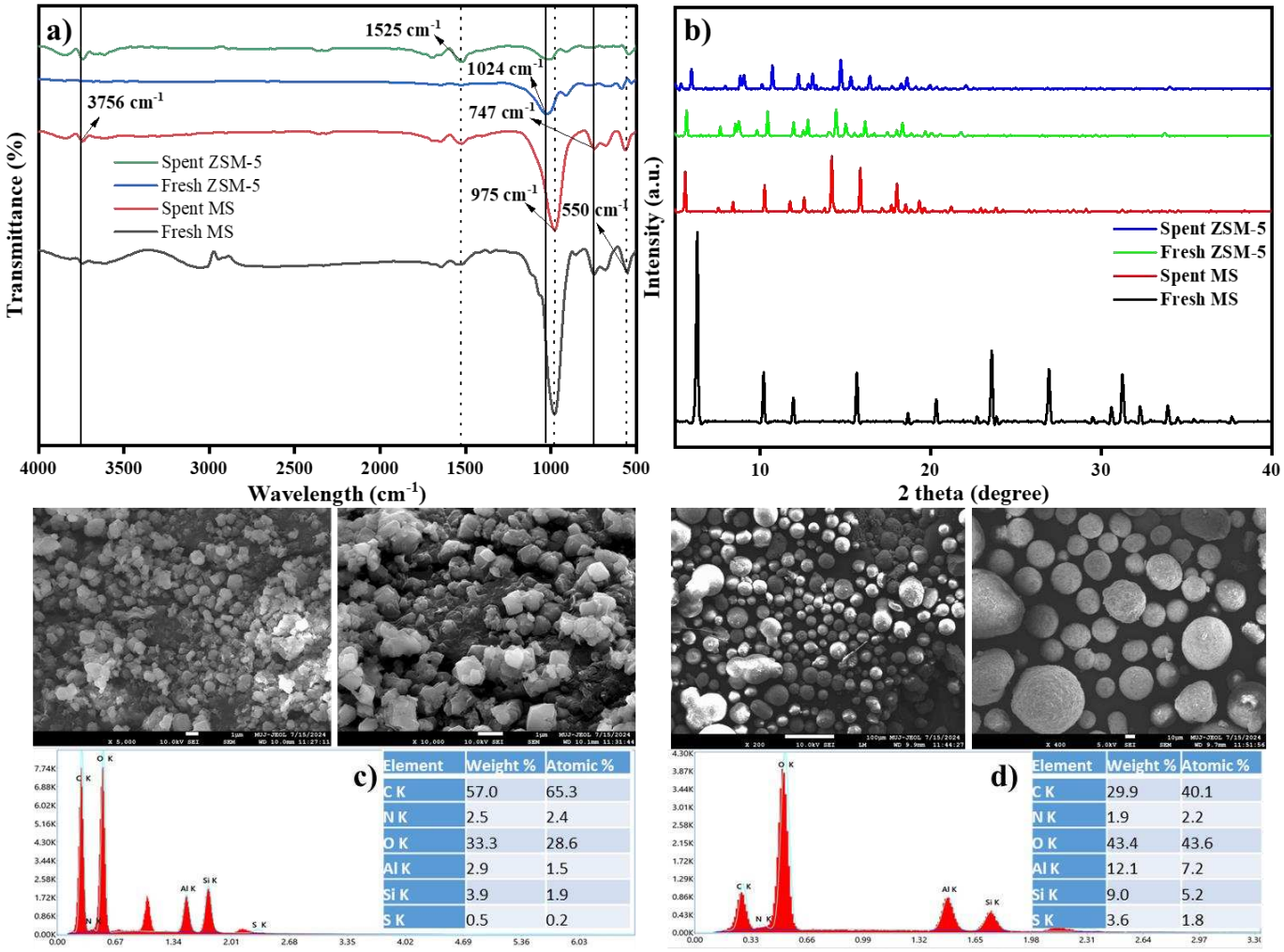

Figure 3: Catalyst Characterization a) FTIR analysis of fresh and spent catalysts b) XRD analysis of fresh and spent catalysts c) SEM and EDX analysis of MS (Molecular Sieve) d) SEM and EDX analysis of ZSM-5

3.3 Pyrolysis product yields:

3.3.1 Effect of co pyrolysis on product yields:

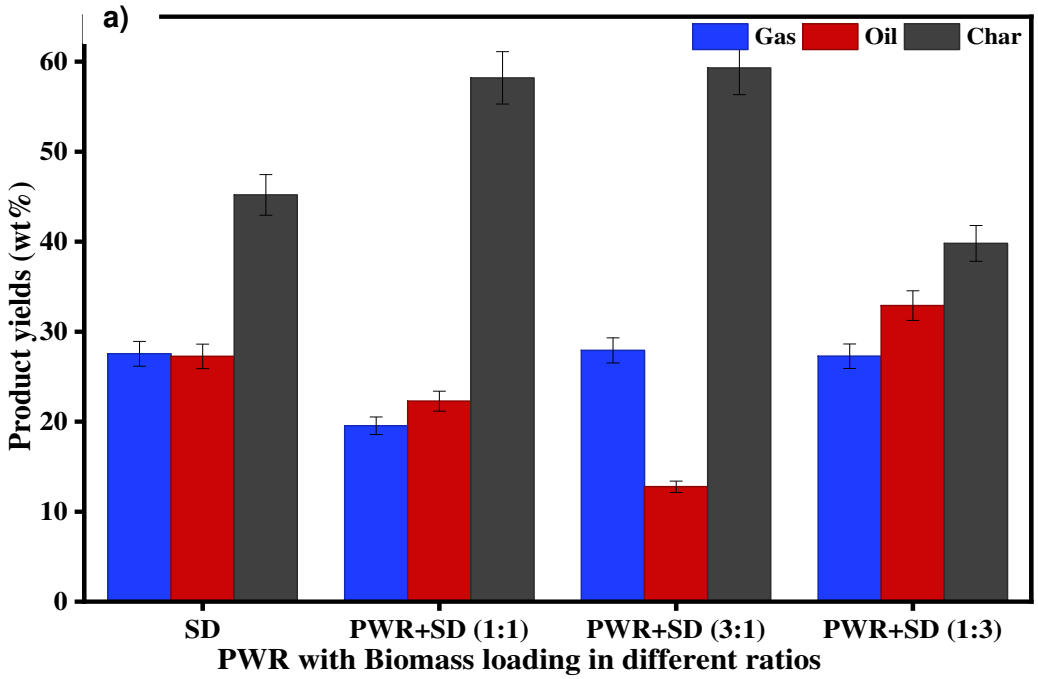

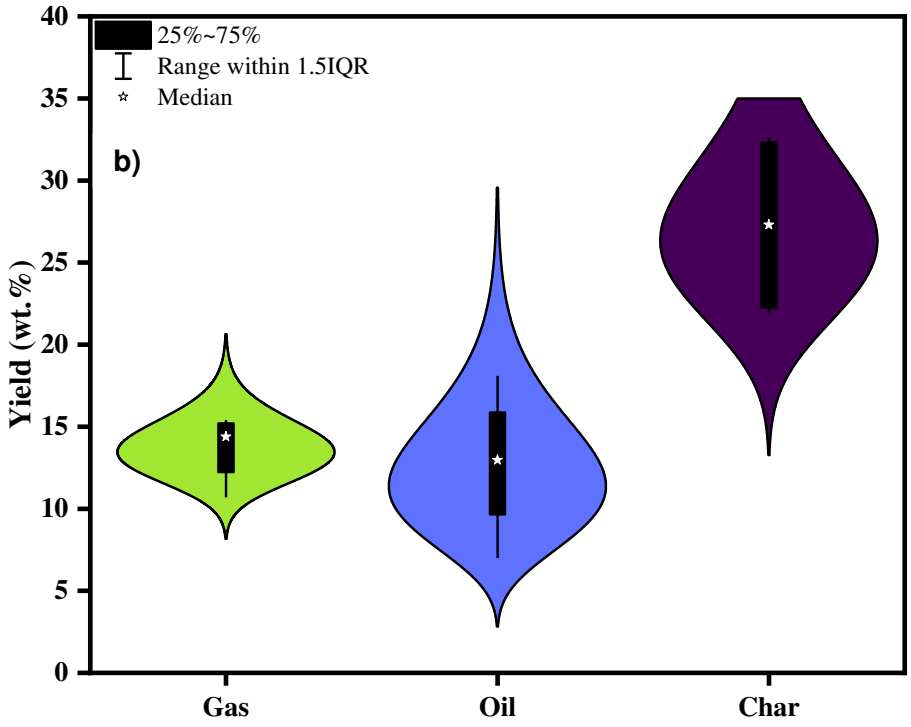

Figure 4: Effect of different blending ratios of SD with PWR on a) pyrolysis product yields and b) Violin plots of pyrolysis product yields

The effect of co-pyrolysis on the product yields (oil, gas, and char) obtained from PWR and SD pyrolysis at varying ratios (1:1, 3:1, 1:3) under non-catalytic conditions is shown in Figure 4. The co-pyrolysis of equal proportions of PWR and SD resulted in higher char yields, with reduced gas and oil yields compared to the pyrolysis of SD alone. At a PWR to SD ratio of 3:1, the oil yield decreased to ~13%, the gas yield showed a slight increase, and the char yield rose to ~60 wt.%. As the proportion of SD increased by up to three times, the oil yield increased to ~33% at 550 °C, while char yield decreased to around ~40%, and gas yield remained at ~27%. This shows that increasing the SD content in the PWR mixture enhanced the condensable, which contributed to the rise in liquid yield.

Pyrolysis of PWR alone under non-catalytic conditions produced negligible liquid yields and led to wax deposition inside the heat exchanger, causing reactor blockage. This wax formation can be attributed to the presence of long-chain hydrocarbons in PWR. Under non-catalytic conditions, the polymer chains in the PWR undergo random cleavage of C-C bonds without being rearranged leading to broad spectrum of waxy compounds. Similar observations of low wax conversions (30.5 %) and oil yields up to 9.3 wt.% were reported to indicate the ineffective thermal cracking[24]. Addressing this issue requires either thermal cracking at higher temperatures or catalytic cracking. In this study, two strategies were employed to mitigate reactor blockages: incorporating SD with PWR and utilizing catalysts.

The influence of varying SD biomass loading on product distribution during the co-pyrolysis of PWR is further illustrated in Figure 4b through violin plots. Gas yields ranged between 8% to 20%, with a median of 14%, indicating that biomass addition had minimal impact on gas production, which was primarily influenced by PWR decomposition. Oil yield exhibited greater variability,

ranging from 2% to 30%, with a median of 13%. Increased biomass contributed to the production of more volatile compounds, likely due to the thermal decomposition cellulose, hemicellulose and lignin present in SD. These observations are in-line with the previous studies with the catalytic co-pyrolysis of refinery oily sludge with biomass where higher oil yields were obtained in the presence of biomass[20]. The greatest variability was observed in char yield, which ranged from 13% to 35%, with a median of 27%. This suggests that PWR significantly influences char formation, leaving more solid residues as observed in Figure 4a. Overall, adding more biomass to PWR enhances oil production but also increases variability in char formation, while gas yields remain relatively stable.

Our results agree with the reported studies in the literature where studies have shown that the pyrolysis of oil palm trunk (OPT), rubberwood sawdust (RWS), and their mixtures at 400–500°C, increased bio-oil yields up to 47 wt.% at higher temperatures due to enhanced decomposition of lignocellulosic components, while biochar yields decreased. RWS produced the highest bio-oil yield, attributed to its high cellulose content and smaller particle size, which improved heat transfer. Co-pyrolysis of OPT with RWS further enhanced bio-oil yields compared to OPT alone[25]. Similar observations of enhanced oil yields were reported with the catalytic co-pyrolysis of sugarcane bagasse (SCB) and HDPE which showed that increasing the HDPE-to-SCB ratio (20:80 to 60:40) improved bio-oil yield (61 to 70 wt.%) and lowering the char formation due to the hydrogen generated during the process. Lower char yields are attributed to the suppression of polymerization and cross-linking reactions in the presence of hydrogen[26]. Co-feeding bagasse with heavy paraffin also significantly reported to increase the bio-oil yields, from 40% for bagasse alone to 52% with paraffin. This highlights paraffin's role as a hydrogen donor, enhancing liquid product formation and reducing solid yields during pyrolysis[27].

3.3.2 Influence of different zeolite catalysts

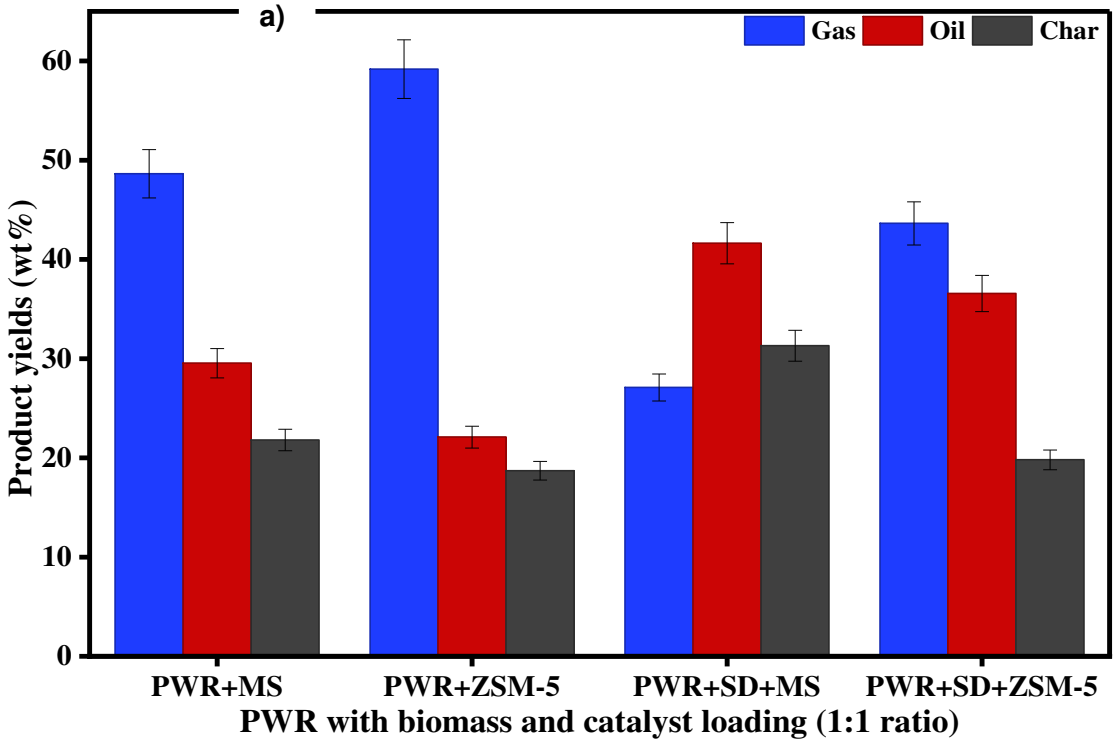

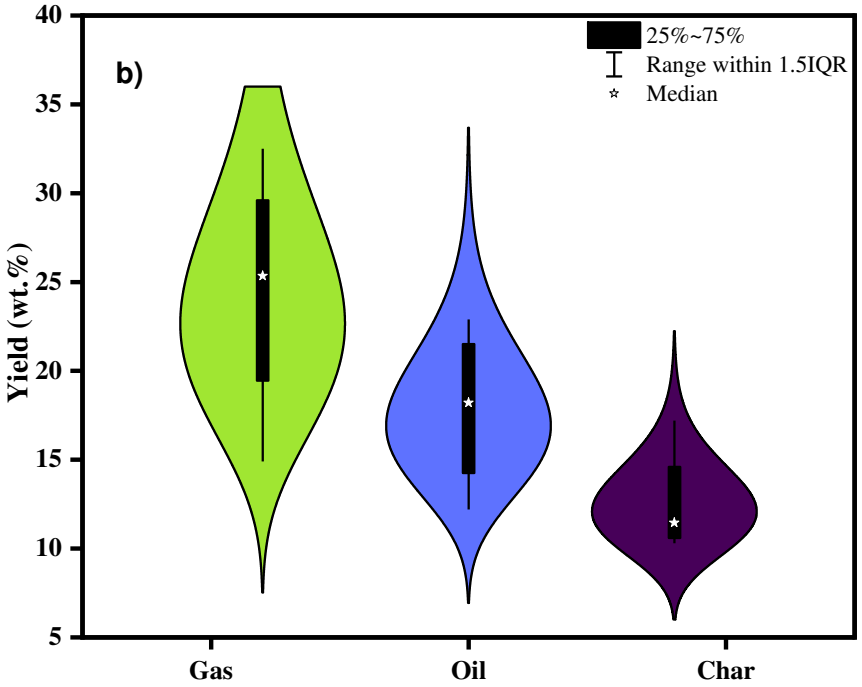

Figure 5: a) Pyrolysis product yields of PWR with SD at a catalyst loading of 1:1 ratio, b) Violin plots of pyrolysis product yields of PWR with and without SD.

343 Preliminary studies into the co-pyrolysis of PWR revealed low liquid product yields, primarily due
344 to the inherent properties of PWR as a feedstock. Additionally, PWR's tendency to form coke or
345 char further limits the yield of valuable liquid and gaseous products. To address challenges such
346 as feedstock clogging, low product yields, and suboptimal product quality, it is necessary to
347 operate at lower pyrolysis temperatures while incorporating suitable catalysts. The use of catalysts
348 facilitates secondary cracking of vapours, enhancing yields and stabilizing liquid products. In
349 addition, the use of catalysts helped reduce reactor blockage by promoting the breakdown of
350 heavier compounds into lighter vapours, improving vapor flow and minimizing sticky residue
351 formation inside the reactor.
352 In this study, molecular sieves (MS) and zeolite (ZSM-5) were employed as *in-situ* catalysts with
353 a feedstock-to-catalyst ratio of 1:1. The product yields obtained under these conditions is presented
354 in Figure 5a and Figure 5b. Zeolite-based catalysts like MS and ZSM-5 are widely recognized in
355 the literature for their effectiveness in vapor-phase upgrading during biomass pyrolysis[18,19,28].
356 As shown in Figure 5a, significant changes in oil yields, char, and gas formation were observed in
357 the presence of zeolite catalysts (MS and ZSM-5). When PWR was premixed with MS at a 1:1
358 ratio, oil and char yields increased, while the gas fraction decreased. The maximum oil yield
359 achieved with MS was approximately 30%. In contrast, the use of ZSM-5 resulted in a reduction
360 in both oil (~22%) and char (~18%) yields, accompanied by a substantial increase in gas
361 production (~59%). This clearly indicates the improved catalytic cracking of ZSM-5 into gaseous
362 products over liquid formation when compared to MS catalysts. Gaseous products from PWR form
363 primarily through chain-end scission during the reaction's initiation phase during which $CH_3^{\bullet}$ and
364 $H^{\bullet}$ radicals are generated, which subsequently react to produce H_2 and CH_4 as termination
365 products. During the early phase of the reaction, primary radicals are generated via random scission

366 which then undergo protonation at Brønsted acid sites or hydride abstraction at Lewis acid sites
367 during the propagation phase, forming carbocations (C_mH_n). The resulting carbocations undergo
368 β-scission, producing smaller hydrocarbons (C_2–C_4) along with CH_4 and H_2[29].
369 Recent studies have also reported similar findings where the use of γ-alumina increased wax
370 conversion to 60.5 wt.% and oil yield to 24.7 wt.%. The oil yields were reported to vary with
371 different zeolites, and it decreased in the order of HY(80)>HY(60)>HZSM-5 (50)>Al_2O_3~HZSM-
372 5 (80). Catalytic hydrocracking of heavy wax using various zeolites achieved wax conversions up
373 to 64.8% with HZSM-5[4]. Larger surface areas, extensive pore volume with appropriate pore size
374 and mild acidity are beneficial for cracking of heavier molecules to lighter liquid molecule
375 inhibiting excessive cracking to gaseous products[30].
376 The results shown in Figure 5a, demonstrate the impact of SD addition and in-situ catalysts on the
377 co-pyrolysis of PWR and SD. The experiments utilized molecular sieves (MS) and zeolite (ZSM-
378 5) as catalysts, with a feedstock-to-catalyst ratio of 1:1. To enhance product yields, PWR was
379 premixed with SD in the presence of MS and ZSM-5 catalysts, and catalytic co-pyrolysis was
380 performed. The addition of SD during catalytic co-pyrolysis significantly increased both oil and
381 char yields, while gas fractions decreased. Specifically, the use of MS resulted in a notable
382 improvement in oil yields. Catalytic co-pyrolysis with ZSM-5 enhanced gas yield with slight
383 reduction in oil yield as compared to MS catalysts as ZSM-5 has strong Brønsted acidity which
384 favours cracking reactions[4,24]. The results indicate that MS performs more effectively in
385 improving product yields when SD is added to the feedstock. As previously discussed, the increase
386 in yield can be attributed to the volatile compounds present in the biomass.
387 The effect of varying catalysts on product distribution during the catalytic co-pyrolysis of PWR
388 and SD with different catalysts (MS and ZSM-5) is further illustrated in Figure 5b through violin

plots. Gas yields ranged from 7% to 35%, with a median of 25%, indicating that catalyst addition significantly impacted gas production, with ZSM-5 having the most pronounced effect. Oil yields varied from 7% to 30%, with a median of 18%. The introduction of MS and biomass contributed to the production of more volatile compounds, likely due to the cellulose and lignin content in SD. The lowest variability was observed in char yield, ranging from 6% to 22%, with a median of 11%. This suggests that the addition of catalysts and biomass facilitates the complete breakdown of heavy compounds in PWR, leading to increased volatile production and a significant reduction in char formation. In general, adding catalysts and biomass to PWR enhances oil production, with MS promoting oil production and ZSM-5 boosting gas production, while minimizing char formation. Table S2 presents a summary of recent literature on both catalytic and non-catalytic conversion of oily sludge residues and plastic wastes.

3.4 Compositional Analysis of Pyrolysis Products

3.4.1 FTIR analysis of feed and pyrolysis products:

The FTIR analysis of the feedstock (PWR) and its pyrolysis product (oil) is presented in Figure 6. The functional groups in the oil composition, derived from varying proportions of SD and different catalysts, were identified through the fingerprint regions of the spectra. No peaks were observed above 3500 cm^{-1}, indicating minimal moisture content in the PWR. A distinct absorption peak at 3745 cm^{-1} corresponds to the O-H stretching vibrations of hydroxyl groups present in the feedstock, likely attributed to SD. Peaks in the range of 2921 cm^{-1} to 2853 cm^{-1} is characteristic of C-H asymmetric and symmetric stretching vibrations, representing CH_3 and CH_2 groups, which are typical in aliphatic hydrocarbons. The prominent peak at 1708 cm^{-1} is indicative of C=O stretching, suggesting the presence of carbonyl compounds, such as aldehydes, ketones, or carboxylic acids. Peaks observed between 1506 cm^{-1} and 1451 cm^{-1} correspond to C=C stretching,

commonly found in aromatic compounds. The peak at 1272 cm^{-1} is associated with the stretching vibrations of -C–O–R bonds, potentially indicating esters or ethers. Furthermore, peaks in the range of 908 cm^{-1} to 719 cm^{-1} can be attributed to stretching vibrations of –NH groups, indicative of nitrogen-containing compounds. These findings highlight the diverse functional groups present in the pyrolysis oil, reflecting the complexity of its chemical composition and the influence of feedstock and catalyst variations on product characteristics.

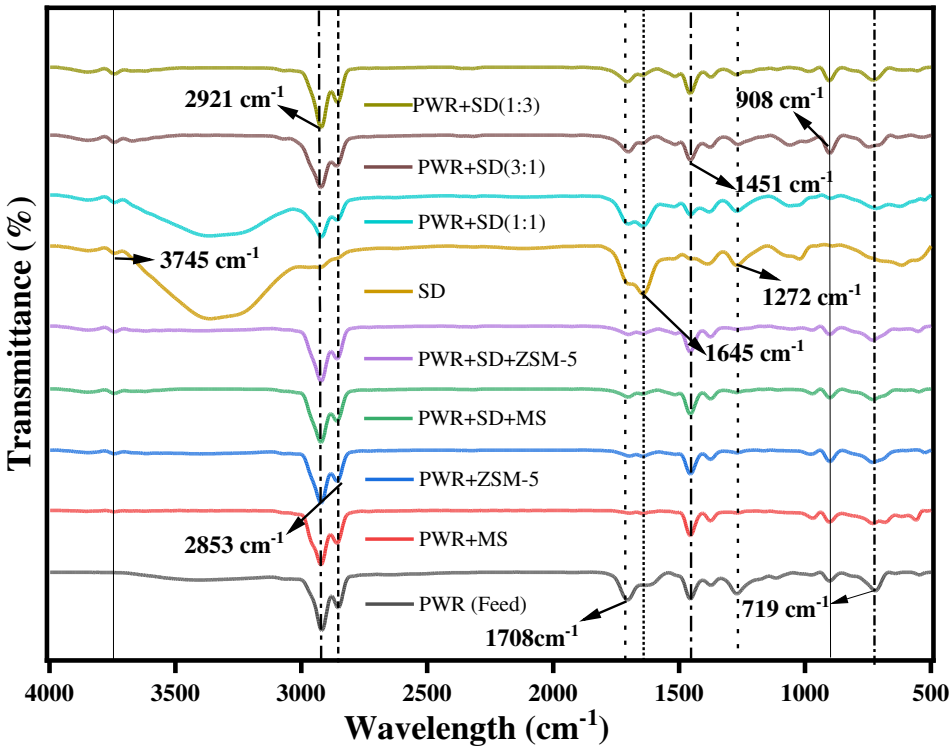

Figure 6: FTIR analysis of PWR feed and their pyrolysis oils obtained at different conditions.

3.4.2 Non-catalytic pyrolysis/co-pyrolysis oil composition analysis:

The composition of pyrolysis oil obtained from PWR under non-catalytic conditions, combined with varying proportions of SD is analysed and presented in Figure 7. The PWR-to-SD ratios considered were 1:1, 1:3, 3:1, and pure SD. The oil derived from pure SD showed high phenolic content (38.0%), comprising compounds such as Phenol, 2-methoxy-, Creosol, Phenol, 4-ethyl-2-methoxy-, and Phenol, 2,6-dimethoxy-. Additionally, significant amounts of ketones (23.3%) were

identified such as Cyclopentanone, 2-Propanone, 1-(acetyloxy)-, 2-Cyclopenten-1-one, 2-methyl-, and 2-Cyclopenten-1-one, 3-methyl-, along with furans (11.3%) including 2-Furancarboxaldehyde, 5-methyl-, and 2-Furanmethanol, tetrahydro-, alcohols (10.2%) like 3,5-Dimethylpyrazole-1-methanol, and acids (5.2%) were also observed. A low proportion of aromatics (3.53%), hydrocarbons (3.17%), aldehydes (0.75%), and other components (4.63%) were present.

In the case of the PWR-to-SD ratio of 1:1, the phenolic content decreased from 38.0% to 21.8%, ketones from 23.3% to 12.2%, alcohols from 10.2% to 9.7%, acids from 5.2% to 1.3%, and aldehydes from 0.75% to zero. Furans slightly decreased from 11.3% to 10.2%, and other components reduced from 4.6% to 2.6%. However, significant increases were noted in aromatics (3.5% to 37.2%) such as Toluene, Benzene 1,2,3-trimethoxy-5-methyl-, and hydrocarbons (3.2% to 5.1%) including 1-Undecene, 1-Heptadecene, and Heneicosane. This indicates that hydrocarbon rich PWR plays a critical role in enhancing aromatic and hydrocarbon production. The decrease in oxygenated compounds such as phenols and acids reflect the partial conversion of these compounds into more thermally stable aromatics and hydrocarbons.

When the PWR-to-SD ratio increased to 1:3, the oil composition revealed an increase in hydrocarbons (35.7%) such as 1-Undecene, 1-Tridecene, and 1-Tetradecene, and ketones (13.8%) including 2-Propanone, 1-(acetyloxy)- and 2-Cyclopenten-1-one, 2-hydroxy-3-methyl-. Furans (13.1%) such as Furfural and 2-Furancarboxaldehyde, 5-methyl-, acids (5.7%) like Benzoic acid, and aldehydes (2.1%) such as Butanal, 2-ethyl-, also increased. Other components rose to 4.7%. In contrast, phenols decreased to 11.8%, aromatics to 6.7%, and alcohols to 6.4%. This suggests that phenolic compounds in SD were converted into hydrocarbons, highlighting the synergistic interaction between PWR and SD during pyrolysis.

For the PWR-to-SD ratio of 3:1, the transformation was even more pronounced, with a hydrocarbon content increase to 69.2%, including compounds like 1-Tridecene, 1-Undecene, and 1-Decene. Alcohols (16.5%) including 1-Octanol, 2-butyl-, 2-Isopropyl-5-methyl-1-heptanol, and 11-Methyldodecanol and aromatics (8.6%) like Toluene, o-Xylene, and Naphthalene also increased, while phenols, ketones, furans, aldehydes, and acids were substantially reduced, reflecting their conversion into hydrocarbons. Other components decreased to 2.1%, likely being transformed into hydrocarbons. The waxy, hydrocarbon-rich nature of PWR likely facilitated these transformations by providing a hydrogen-rich environment for the cracking and deoxygenation of SD-derived intermediates. These findings confirm that PWR serves as a promising feedstock for hydrocarbon production. However, its direct use is limited due to its semi-solid, waxy nature, which can cause operational issues such as reactor choking. To overcome this, blending of biomass along with PWR enhances process efficiency by facilitating a more uniform thermal conversion and synergistic interactions during co-pyrolysis.

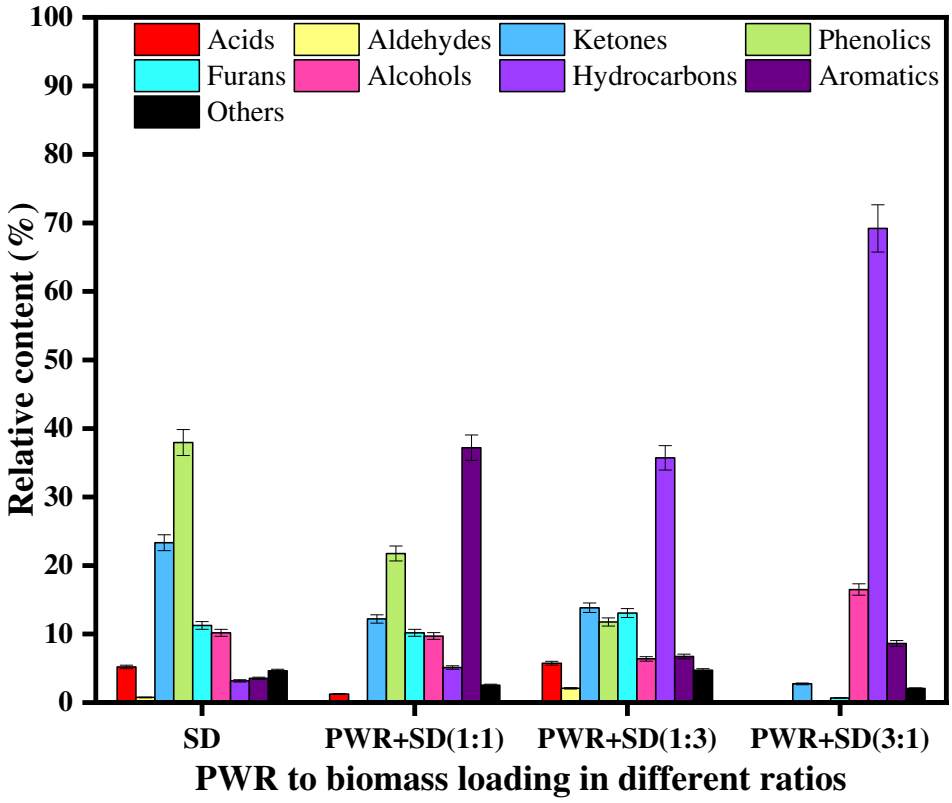

Figure 7: Pyrolytic oil composition derived from the co-pyrolysis of PWR and SD with different proportions.

3.4.3 Catalytic pyrolysis/co-pyrolysis oil composition analysis:

The composition of pyrolysis and co-pyrolysis oil obtained under catalytic conditions using MS and ZSM-5 is shown in Figure 8. For the PWR-to-MS ratio of 1:1, the pyrolysis oil consisted of high hydrocarbon content (78.7%) including 1-Tridecene, Hexadecane, 1-Undecene, Octane, and 1-Decene. Aromatic compounds such as Toluene, Ethylbenzene, and o-Xylene were present in lower amounts, along with (9.0%) alcohols (8.0%) like 1-Heptanol, 2,4-diethyl-, and 9-Octadecenol, and other components (3.1%). Functional compounds such as acids, aldehydes, ketones, phenols, and furans were nearly negligible (<1%). This indicates that MS effectively facilitates the conversion of PWR into hydrocarbons.

In contrast, when ZSM-5 was used with PWR, the hydrocarbon content decreased from 78.7% to 65.9%. Simultaneously the proportions of alcohols increased from 8.0% to 14.7%, aromatics from

9.0% to 13.7%, and other components from 3.1% to 4.5%. This suggests that ZSM-5 promotes the formation of oxygenated compounds and aromatics during pyrolysis. The differences in the catalytic activity of MS and ZSM-5 can be attributed to their distinct pore structures and acidity. Literature studies have shown that ZSM-5, due to its high acidity and shape-selective properties, enhances the formation of aromatic hydrocarbons and oxygenated compounds, whereas MS tend to favour the production of hydrocarbons with minimal oxygenated by-products[31]. Catalysts with mild acidity and moderate pore sizes facilitate the formation of short-chain paraffins and olefins. In contrast, highly acidic catalysts with smaller pore sizes enhance the conversion of olefins and paraffins into aromatic compounds by promoting Diels-Alder reactions, cyclization, isomerization, and dehydrogenation[32]. Paraffins are transformed into aromatics through dehydrogenation and cyclization, driven by the synergistic interaction between Lewis and Brønsted acid sites. Additionally, in the Diels-Alder reaction, Brønsted acid sites promote protonation of olefinic groups, leading to the formation of olefinic carbonium ions. These intermediates subsequently undergo isomerization, yielding naphthenic hydrocarbons which can undergo dehydrogenation reactions at the Lewis acid sites forming aromatics and hydrogen[33,34].

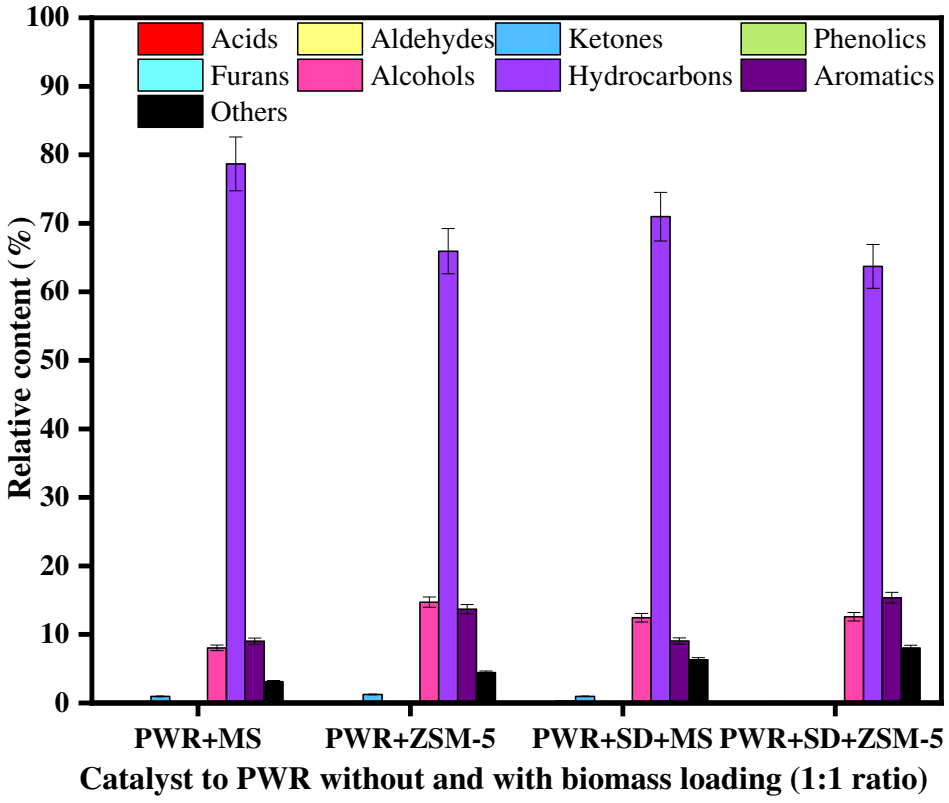

Figure 8: Pyrolytic oil composition derived from catalytic pyrolysis of PWR and co-pyrolysis of PWR with SD and PWR using different catalysts.

Under catalytic co-pyrolysis conditions, using SD and PWR with MS and ZSM-5 in ([1:1]:1) ([PWR:SD]:CAT) ratios, the oil composition showed significant variation as presented in Figure 8. Upon the addition of SD in a 1:1 ratio, the hydrocarbon content decreased to 71%, while alcohols (12.4%) and other components (6.3%) increased, with aromatics (9.0%) remaining relatively constant. This indicates that biomass addition influences the conversion pathway, leading to higher oxygenated compounds. When ZSM-5 was used, a more pronounced decrease in hydrocarbon content (63.7%) was observed. Simultaneously, the proportions of alcohols (12.6%), aromatics (15.4%), and other components (8.0%) increased. Notably, furans, which were slightly present under non-catalytic conditions and with MS catalysis, completely disappeared with ZSM-5. This suggests that ZSM-5 facilitates the complete transformation of furans into other compounds. These findings demonstrate that the addition of biomass during catalytic pyrolysis reduces the

hydrocarbon content while increasing alcohol and aromatic content. This effect is more significant with ZSM-5, owing to its higher acidity and selective catalytic properties.

3.5 Carbon number distribution of pyrolytic oil from catalytic co-pyrolysis of PWR with SD:

The carbon number distribution of the pyrolytic oil was grouped into different fractions ranging from C_6–C_{10}, C_{11}–C_{15}, C_{16}–C_{20}, C_{21}–C_{25}, C_{26}–C_{30}, C_{31}–C_{35}, and > C_{35} and it is presented in Figure 9a and b. The catalytic pyrolysis of PWR with MS catalyst, mainly consisted of lighter fractions with C_6–C_{10} accounting up to 34.4%, while C_{11}–C_{15} and C_{16}–C_{20} compounds accounted for 36.7% and 20.8%, respectively with an overall composition being in the range of (C_6–C_{20}) represented 91.9% of the total oil composition. In contrast, the heavier fractions, including C_{21}–C_{25} (5.1%), C_{26}–C_{30} (0.73%), and C_{31}–C_{35} (0.99%), comprised only 6.8% of the total composition. The oil composition of PWR with ZSM-5 catalyst exhibited a distinct distribution across various chemical fractions. The major fractions were found to be C_6–C_{10} (27.6%), C_{11}–C_{15} (40.1%), and C_{16}–C_{20} (20.9%), together accounted for 88.6% of the total oil composition. Compared to MS catalyst, a slight increase in the heavier fractions was observed, with C_{21}–C_{25} compounds contributing 6.9%, C_{26}–C_{30} compounds at 2.9%, C_{31}–C_{35} compounds at 1.4%, and > C_{35} compounds at 0.2%, collectively making up 11.4% of the composition.

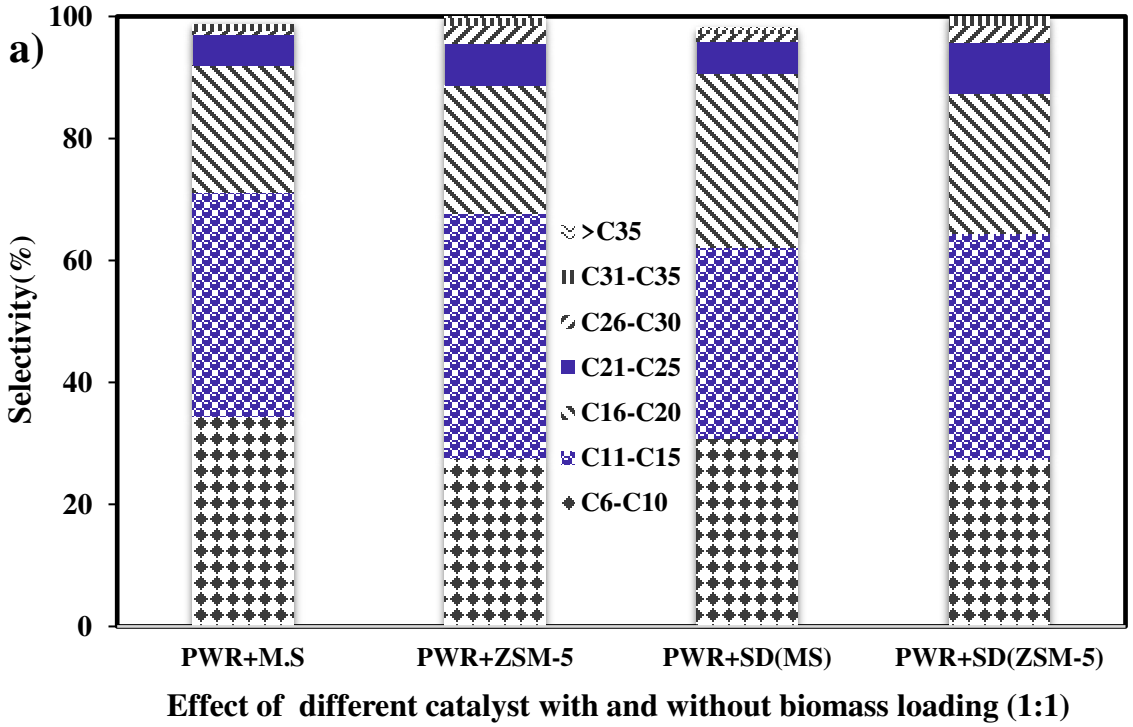

522

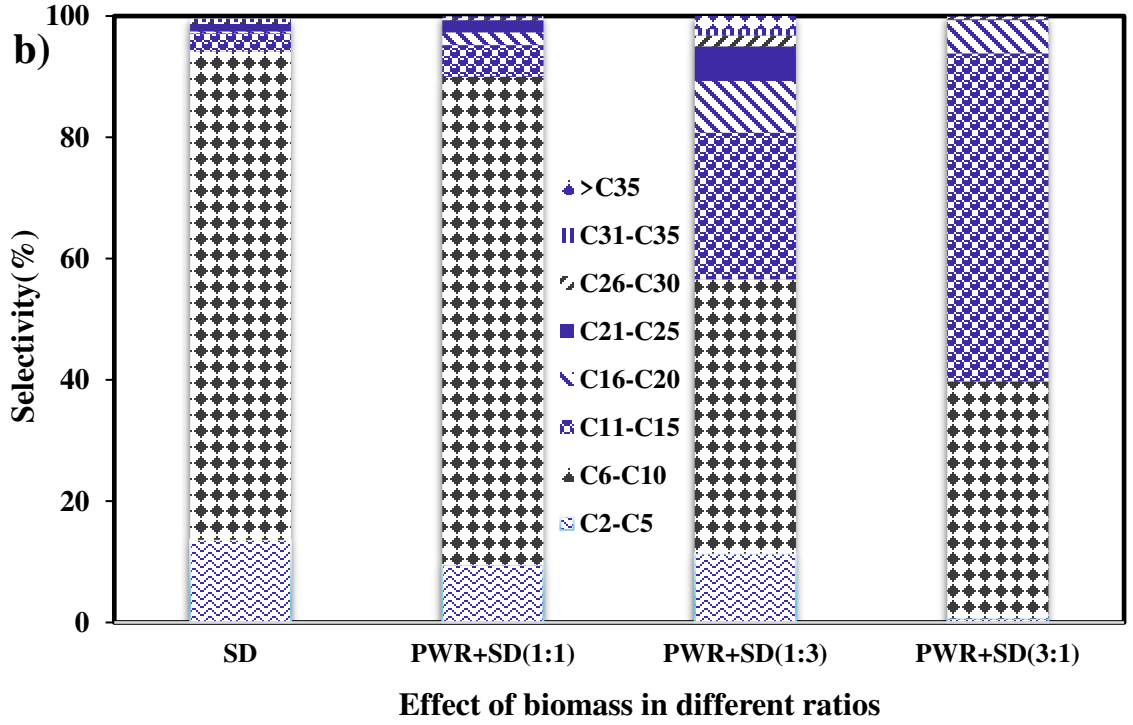

523

524 *Figure 9: Carbon number distribution of oils produced from* ***a)*** *pyrolysis of PWR and different catalysts*
525 *(MS, ZSM-5) and PWR with SD (1:1) with catalysts* ***b)*** *catalytic co-pyrolysis of PWR and SD.*

The influence of different catalysts in combination with PWR and biomass on carbon number distribution is depicted in Figure 9a. Catalytic co-pyrolysis with molecular sieve catalysts resulted in significant amount of lighter fractions made up a significant portion of the pyrolytic oil. Specifically, C_6–C_{10} compounds accounted for 30.8%, while C_{11}–C_{15} and C_{16}–C_{20} compounds represented 31.3% and 28.6%, respectively. Combined, the fractions of C_6–C_{20} constituted up to 90.6% of the oil composition. In contrast, the heavier fractions, including C_{21}–C_{25} (5.3%), C_{26}–C_{30} (1.3%), C_{31}–C_{35} (0.8%), and > C_{35} (0.21%), contributed only 9.4% to the total composition.

In the case of PWR with SD and ZSM-5, the oil composition exhibited a distinct distribution among the fractions. The fractions comprising of C_6–C_{10} (27.5%), C_{11}–C_{15} (37.0%), and C_{16}–C_{20} (22.9%), collectively made up 87.4% of the total oil composition. Compared with a MS catalyst, a slight increase in the heavier fractions was observed with C_{21}–C_{25} compounds contributing 8.3%, C_{26}–C_{30} compounds at 2.9%, and C_{31}–C_{35} compounds at 1.6%, together accounting up to 12.6% of the total composition.

The effect of different blending ratios of biomass with PWR on the carbon number distribution is shown in Figure 9b. For SD, the lighter fractions constituted a significant portion of the pyrolytic oil. mainly consisting of C_2–C_5 up to 13.6%, and C_6–C_{10} compounds of 80.6%, while C_{11}–C_{15} compounds represented 2.97%, and C_{16}–C_{20} compounds contributed to 0.33%. Together, the light fractions (C_2–C_{20}) constituted 97.5% of the total oil composition. In contrast, the heavier fractions, including C_{21}–C_{25} (1.24%), C_{26}–C_{30} (0.31%), and C_{31}–C_{35} (0.51%), collectively contributed only 2.53% to the overall composition.

For PWR and SD mixed at a 1:1 ratio, the pyrolytic oil remained rich in lighter hydrocarbons. The C_2–C_5 fraction constituted 9.5%, while the C_6–C_{10} fraction was dominant at 80.6%. The C_{11}–C_{15} and C_{16}–C_{20} fractions accounted for 5.2% and 2.1%, respectively, leading to a combined light

fraction (C_2–C_{20}) of 97.4%. The heavier fractions were minimal, with C_{21}–C_{25} at 2.01%, C_{26}–C_{30} at 0.34%, and >C_{35} at 0.3%, collectively comprising only 2.6%.

At a 1:3 PWR-to-SD ratio, the oil composition exhibited notable variations. The C_2–C_5 fraction increased to 11.4%, while the C_6–C_{10} fraction decreased to 45.2%. The C_{11}–C_{15} and C_{16}–C_{20} fractions contributed 24.2% and 8.6%, respectively, bringing the total light fractions (C_2–C_{20}) to 89.3%. Concurrently, a slight increase in heavier fractions was observed, with C_{21}–C_{25} at 5.73%, C_{26}–C_{30} at 1.8%, and >C_{35} at 2.2%, collectively accounting for 10.7%. These findings indicate a shift towards heavier hydrocarbons with an increasing SD ratio.

For a 3:1 PWR-to-SD ratio, the oil composition exhibited a noticeable shift. The C_2–C_5 fraction declined to 0.67%, and the C_6–C_{10} fraction decreased to 39.09%. Conversely, the C_{11}–C_{15} fraction increased significantly to 54.1%, while the C_{16}–C_{20} fraction contributed 5.5%, leading to a total light fraction (C_2–C_{20}) of 99.3%. The heavier fractions also showed a reduction, with C_{21}–C_{25} at 0.13%, C_{26}–C_{30} at 0.37%, and >C_{35} at 0.15%, collectively contributing only 0.67%. This distribution highlights the dominance of lighter hydrocarbons at this ratio, with minimal formation of heavier fractions.

3.6 Char characterization

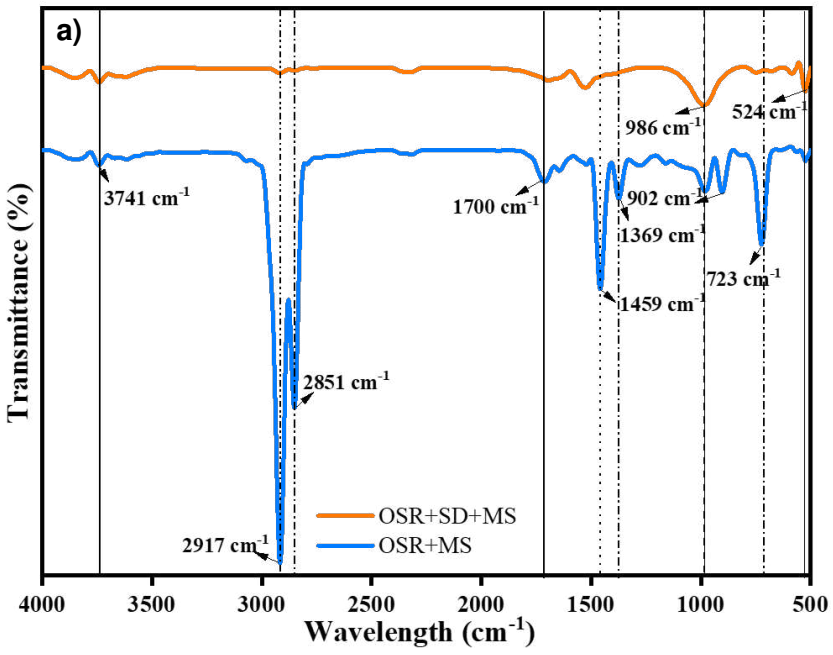

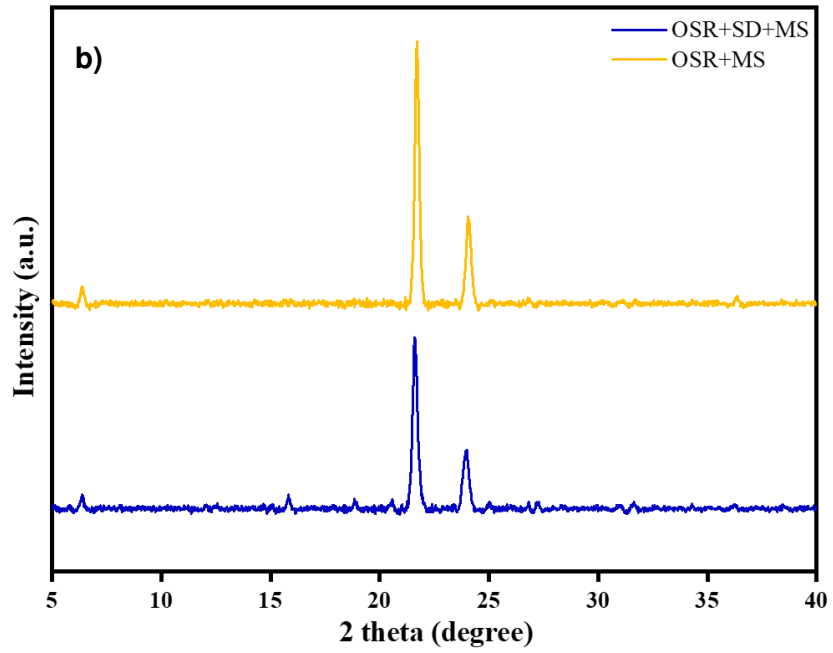

Figure 3: Char characterization using a) FTIR and b) XRD analysis.

The char derived from the catalytic pyrolysis of PWR and catalytic co-pyrolysis of PWR with SD in the presence of MS catalyst was analysed using FTIR and XRD analysis to determine the functional groups as well as in identifying the crystallinity is presented in Figure 10 a & b. The

572 FTIR analysis of the char obtained from catalytic pyrolysis of PWR and co-pyrolysis of PWR with
573 SD were found to be significantly different that can be attributed mainly due to the feed stock
574 characteristics. The char from PWR revealed several multiple peaks at 3741, 2917, 2851, 1700,
575 1459, 1369, 986, 902, and 723 cm^{-1} while the char from PWR with SD showed significantly less
576 number of peaks observed at 3741, 1470, 986, and 524 cm^{-1} indicating a smaller fingerprint region
577 compared to PWR + MS and these are identical with the oil composition from pyrolysis.
578 The XRD patterns of the char (PWR with SD and MS, PWR along MS) are presented in Figure 10
579 b highlighting multiple peaks that confirm the crystalline nature of the materials. The chars derived
580 from PWR and PWR with SD were found to similar crystalline behaviour where the prominent
581 diffraction peaks from PWR with SD were found to have a 2θ values of 6.44°, 21.74°, 24.08°, and
582 36.45° while, similar in comparison, the char of PWR along MS exhibited peaks at 6.50°, 15.82°,
583 21.68°, and 23.85°.

4. Conclusion

This study investigated the thermochemical conversion of PWR through catalytic and non-catalytic co-pyrolysis with sawdust (SD) to maximize the production of liquid fuels, particularly naphtha and diesel-range hydrocarbons, supporting a circular economy. Thermal decomposition kinetics showed that PWR volatilizes predominantly below 500 °C without char formation and has an activation energy of 31–39 kJ mol^{-1}. Co-pyrolysis with SD significantly influenced product yields and quality. A lower PWR ratio (1:3 PWR:SD) improved overall liquid yields, while a higher PWR ratio (3:1) increased hydrocarbon 69.2% and reduced oxygenates such as phenols, acids, and ketones. Product distribution varied with feed ratios, with higher SD content favoring heavier hydrocarbons (C21–C35, 10.7%), while a 3:1 PWR-to-SD ratio promoted mid-range hydrocarbons (C11–C15, 54.1%) with minimal heavy fractions (0.67%). Catalytic pyrolysis using molecular sieves (MS) outperformed ZSM-5, providing higher liquid yields and better hydrocarbon selectivity. Specifically, catalytic pyrolysis of PWR with MS at a 1:1 ratio achieved a hydrocarbon yield of 78.7% and an oil yield of 30%, while catalytic co-pyrolysis of PWR:SD:MS (1:1:1) achieved 71% hydrocarbon yield with 42% oil yield. Although catalyst regeneration studies were not performed due to limited feedstock, a follow-up study is ongoing in this direction. This work provides valuable insights into sustainable fuel production from plastic-derived residues and offers a practical approach for efficient waste-to-fuel conversion.

Acknowledgements:

The authors thank the Manipal University Jaipur (MUJ) for providing access to the Central Analytical Facilities (CAF) and Sophisticated Analytical Instrumentation Facility (SAIF). Additionally, the authors also acknowledge the SAIF facility at IIT Bombay for conducting the CHNS analysis of the samples. The authors also acknowledge Dr. Abhishek Sharma and Dr. Sivasankar Kakku for providing the PWR obtained from the Waste to Resources Laboratory.

Credit authorship statement:

Himanshi Sharma: Methodology, Investigation, Data curation, Formal analysis, Writing – original draft

Nandana Chakinala: Formal analysis, Supervision, Writing – review & editing

Chiranjeevi Thota: Resources, Writing – review & editing

Daya Pandey: Writing – review & editing

Anand Gupta Chakinala: Writing – review & editing, Formal analysis, Validation, Supervision, Resources, Project administration

Funding:

No funding was received for conducting this study.

References

[1] M.J.B. Kabeyi, O.A. Olanrewaju, Review and Design Overview of Plastic Waste-to-Pyrolysis Oil Conversion with Implications on the Energy Transition, Journal of Energy 2023 (2023). https://doi.org/10.1155/2023/1821129.

[2] M. Okan, H.M. Aydin, M. Barsbay, Current approaches to waste polymer utilization and minimization: a review, Journal of Chemical Technology and Biotechnology 94 (2019) 8–21. https://doi.org/10.1002/jctb.5778.

[3] K. Ragaert, L. Delva, K. Van Geem, Mechanical and chemical recycling of solid plastic waste, Waste Management 69 (2017) 24–58. https://doi.org/10.1016/j.wasman.2017.07.044.

[4] I.H. Choi, H.J. Lee, G.B. Rhim, D.H. Chun, K.H. Lee, K.R. Hwang, Catalytic hydrocracking of heavy wax from pyrolysis of plastic wastes using Pd/Hβ for naphtha-ranged hydrocarbon production, J Anal Appl Pyrolysis 161 (2022) 105424. https://doi.org/10.1016/j.jaap.2021.105424.

[5] M.M. Hasan, R. Haque, M.I. Jahirul, M.G. Rasul, Pyrolysis of plastic waste for sustainable energy Recovery: Technological advancements and environmental impacts, Energy Convers Manag 326 (2025) 119511. https://doi.org/10.1016/J.ENCONMAN.2025.119511.

[6] D.M. Zairin, M.P. Ruiz, S.R.A. Kersten, Pyrolysis of Polyethylene: Chemical Kinetics, Mass Transfer, and Reflux System, Energy & Fuels 39 (2025) 1015–1025. https://doi.org/10.1021/acs.energyfuels.4c05204.

[7] M. Monzavi, Z. Chen, A. Solouki, J. Chaouki, Microwave-assisted catalytic pyrolysis of paraffin wax, Fuel 320 (2022) 123886. https://doi.org/10.1016/j.fuel.2022.123886.

[8] E. Rodríguez, A. Gutiérrez, R. Palos, F.J. Vela, J.M. Arandes, J. Bilbao, Fuel production by cracking of polyolefins pyrolysis waxes under fluid catalytic cracking (FCC) operating conditions, Waste Management 93 (2019) 162–172. https://doi.org/10.1016/j.wasman.2019.05.005.

[9] J.L. Hodala, J.S. Jung, E.H. Yang, G.H. Hong, Y.S. Noh, D.J. Moon, Hydrocracking of FT-wax to fuels over non-noble metal catalysts, Fuel 185 (2016) 339–347. https://doi.org/10.1016/j.fuel.2016.07.124.

[10] P. Lovás, P. Hudec, B. Jambor, E. Hájeková, M. Horňáček, Catalytic cracking of heavy fractions from the pyrolysis of waste HDPE and PP, Fuel 203 (2017) 244–252. https://doi.org/10.1016/j.fuel.2017.04.128.

[11] M. Alam, A. Bhavanam, A. Jana, J. kumar S. Viroja, N.R. Peela, Co-pyrolysis of bamboo sawdust and plastic: Synergistic effects and kinetics, Renew Energy 149 (2020) 1133–1145. https://doi.org/10.1016/J.RENENE.2019.10.103.

[12] K.G. Burra, A.K. Gupta, Kinetics of synergistic effects in co-pyrolysis of biomass with plastic wastes, Appl Energy 220 (2018) 408–418. https://doi.org/10.1016/J.APENERGY.2018.03.117.

[13] C. Kassargy, S. Awad, G. Burnens, K. Kahine, M. Tazerout, Experimental study of catalytic pyrolysis of polyethylene and polypropylene over USY zeolite and separation

to gasoline and diesel-like fuels, J Anal Appl Pyrolysis 127 (2017) 31–37. https://doi.org/10.1016/J.JAAP.2017.09.005.

[14] A. Marcilla, M.I. Beltrán, R. Navarro, Thermal and catalytic pyrolysis of polyethylene over HZSM5 and HUSY zeolites in a batch reactor under dynamic conditions, Appl Catal B 86 (2009) 78–86. https://doi.org/10.1016/J.APCATB.2008.07.026.

[15] S.M. Al-Salem, A. Antelava, A. Constantinou, G. Manos, A. Dutta, A review on thermal and catalytic pyrolysis of plastic solid waste (PSW), J Environ Manage 197 (2017) 177–198. https://doi.org/10.1016/J.JENVMAN.2017.03.084.

[16] E.P. da Silva, V.H. Fragal, E.H. Fragal, T. Sequinel, L.F. Gorup, R. Silva, E.C. Muniz, Sustainable energy and waste management: How to transform plastic waste into carbon nanostructures for electrochemical supercapacitors, Waste Management 171 (2023) 71–85. https://doi.org/10.1016/J.WASMAN.2023.08.028.

[17] S. Kakku, N. Jonna, A.G. Chakinala, J. Joshi, R. Vinu, C. Thota, A. Sharma, Co-Pyrolysis Studies of Agricultural Residue and Plastics for Process Optimization in a Rotary Kiln Reactor System, Ind Eng Chem Res 63 (2024) 21816–21830. https://doi.org/10.1021/acs.iecr.4c03309.

[18] R. Singh, S. Kakku, K. Shah, X. Zhang, A. Sharma, N. Chakinala, A.G. Chakinala, Catalytic pyrolysis of torrefied biomass with molecular sieve catalysts to produce hydrocarbon rich biocrude, Environ Prog Sustain Energy (2024). https://doi.org/10.1002/ep.14446.

[19] R. Singh, N. Chakinala, K. Mohanty, A.G. Chakinala, Catalytic upgrading of biomass pyrolysis vapors for selective production of phenolic monomers over metal oxide modified alumina catalysts, J Environ Chem Eng 11 (2023) 111518. https://doi.org/10.1016/j.jece.2023.111518.

[20] H. Sharma, R. Singh, N. Chakinala, S. Majumder, C. Thota, A.G. Chakinala, Co-pyrolysis of refinery oil sludge with biomass and spent fluid catalytic cracking catalyst for resource recovery, Environmental Science and Pollution Research 31 (2024) 52086–52104. https://doi.org/10.1007/s11356-024-34630-x.

[21] H. Sharma, R. Singh, N. Chakinala, S. Majumder, C. Thota, A.G. Chakinala, Co-pyrolysis of refinery oil sludge with biomass and spent fluid catalytic cracking catalyst for resource recovery, Environmental Science and Pollution Research 31 (2024) 52086–52104. https://doi.org/10.1007/s11356-024-34630-x.

[22] H.K. Balsora, S. Kartik, T.J. Rainey, A. Abbas, J.B. Joshi, A. Sharma, A.G. Chakinala, Kinetic modelling for thermal decomposition of agricultural residues at different heating rates, Biomass Convers Biorefin 13 (2023) 3281–3295. https://doi.org/10.1007/s13399-021-01382-4.

[23] I.B. Dauda, M. Yusuf, S. Gbadamasi, M. Bello, A.Y. Atta, B.O. Aderemi, B.Y. Jibril, Highly Selective Hierarchical ZnO/ZSM-5 Catalysts for Propane Aromatization, ACS Omega 5 (2020) 2725–2733. https://doi.org/10.1021/acsomega.9b03343.

[24] H. Yim, S. Valizadeh, K. Cho, Y.K. Park, Production of low-aromatic oil from catalytic pyrolysis of waste plastics-derived wax, J Anal Appl Pyrolysis 186 (2025) 106964. https://doi.org/10.1016/j.jaap.2025.106964.

[25] P. Sakulkit, A. Palamanit, R. Dejchanchaiwong, P. Reubroycharoen, Characteristics of pyrolysis products from pyrolysis and co-pyrolysis of rubber wood and oil palm

trunk biomass for biofuel and value-added applications, J Environ Chem Eng 8 (2020) 104561. https://doi.org/10.1016/j.jece.2020.104561.

[26] H. Hassan, J.K. Lim, B.H. Hameed, Catalytic co-pyrolysis of sugarcane bagasse and waste high-density polyethylene over faujasite-type zeolite, Bioresour Technol 284 (2019) 406–414. https://doi.org/10.1016/j.biortech.2019.03.137.

[27] M. Kouhi, K. Shams, Bulk features of catalytic co-pyrolysis of sugarcane bagasse and a hydrogen-rich waste: The case of waste heavy paraffin, Renew Energy 140 (2019) 970–982. https://doi.org/10.1016/j.renene.2019.03.115.

[28] H. Sharma, R. Singh, N. Chakinala, S. Majumder, C. Thota, A.G. Chakinala, Co-pyrolysis of refinery oil sludge with biomass and spent fluid catalytic cracking catalyst for resource recovery, Environmental Science and Pollution Research 31 (2024) 52086–52104. https://doi.org/10.1007/s11356-024-34630-x.

[29] Y. Zhang, Z. Fu, W. Wang, G. Ji, M. Zhao, A. Li, Kinetics, Product Evolution, and Mechanism for the Pyrolysis of Typical Plastic Waste, ACS Sustain Chem Eng 10 (2022). https://doi.org/10.1021/acssuschemeng.1c04915.

[30] L. Dai, N. Zhou, Y. Lv, K. Cobb, Y. Cheng, Y. Wang, Y. Liu, P. Chen, R. Zou, H. Lei, R. Ruan, Pyrolysis-catalysis for waste polyolefin conversion into low aromatic naphtha, Energy Convers Manag 245 (2021). https://doi.org/10.1016/j.enconman.2021.114578.

[31] N. Chakinala, A.G. Chakinala, Process Design Strategies to Produce p-Xylene via Toluene Methylation: A Review, Ind Eng Chem Res 60 (2021) 5331–5351. https://doi.org/10.1021/acs.iecr.1c00625.

[32] L. Dai, N. Zhou, Y. Lv, K. Cobb, P. Chen, Y. Wang, Y. Liu, R. Zou, H. Lei, B.A. Mohamed, R. Ruan, Y. Cheng, Catalytic reforming of polyethylene pyrolysis vapors to naphtha range hydrocarbons with low aromatic content over a high silica ZSM-5 zeolite, Science of the Total Environment 847 (2022). https://doi.org/10.1016/j.scitotenv.2022.157658.

[33] X. Zhang, H. Lei, G. Yadavalli, L. Zhu, Y. Wei, Y. Liu, Gasoline-range hydrocarbons produced from microwave-induced pyrolysis of low-density polyethylene over ZSM-5, Fuel 144 (2015) 33–42. https://doi.org/10.1016/j.fuel.2014.12.013.

[34] M.S. Abbas-Abadi, Y. Ureel, A. Eschenbacher, F.H. Vermeire, R.J. Varghese, J. Oenema, G.D. Stefanidis, K.M. Van Geem, Challenges and opportunities of light olefin production via thermal and catalytic pyrolysis of end-of-life polyolefins: Towards full recyclability, Prog Energy Combust Sci 96 (2023). https://doi.org/10.1016/j.pecs.2022.101046.

Declaration of interests

☒The authors declare that they have no known competing financial interests or personal relationships that could have appeared to influence the work reported in this paper.

☐The authors declare the following financial interests/personal relationships which may be considered as potential competing interests: